

RESEARCH ARTICLE

Fuzzy TSMCSPO for Trajectory Tracking of Nuclear Reactor Dismantlement Robot Manipulator

CHENGQIAN LI^{ID}, HAMZA KHAN^{ID}, JINWON LEE, JAEHYUNG KIM^{ID},
AND MIN CHEOL LEE^{ID}, (Member, IEEE)

School of Mechanical Engineering, Pusan National University, Geumjeong-gu, Busan 46241, South Korea

Corresponding author: Min Cheol Lee (mcleee@pusan.ac.kr)

This work was supported by Korea Institute for Advancement of Technology (KIAT) grant funded by the Korean Ministry of Trade, Industry and Energy (MOTIE) (P0008473, Human Resource Development (HRD) Program for Industrial Innovation).

ABSTRACT In this study, a fuzzy logic system to tune the parameters of terminal sliding mode control with a sliding perturbation observer (TSMCSPO) in real-time is proposed according to the system's state changes to improve the control performance of TSMCSPO for a 5-DOF robot manipulator used for nuclear reactor dismantlement. Accurate trajectory tracking control is required when using a multi-DOF robot manipulator to cut the decommissioned nuclear reactor. A TSMCSPO scheme using TSMC in SPO has been proposed in previous research, which improves the estimation and convergence performance of traditional SMCSPO. In TSMCSPO, the parameters of the controller are important to enhance the control performance. Moreover, due to the influence of the working environment and the uncertainty of the system, the characteristics of the system will be changed during the trajectory tracking control of the multi-degree-of-freedom robot manipulator. Therefore, real-time optimal parameter tuning is required. In this regard, using fuzzy logic to tune the parameters is an effective method. By designing fuzzy rules, the controller parameters can be optimized. In this study, the proposed algorithm and, the trajectory tracking control simulation of the robot manipulator in the nuclear reactor vessel internal (RVI) are implemented in MATLAB/Simulink environment. The control algorithm is verified by the experiments on a real robot manipulator platform. The outstanding control performance of the algorithm is demonstrated by comparing the trajectory tracking error between the proposed fuzzy TSMCSPO scheme and TSMCSPO with fixed parameters.

INDEX TERMS Terminal sliding mode control (TSMC), sliding perturbation observer (SPO), decommissioning of nuclear facilities, fuzzy logic system, parameter tuning, perturbation estimation.

I. INTRODUCTION

In the next few decades, a large number of nuclear power plants (NPPs) will be retired from service, and decommissioning of old nuclear facilities is a crucial issue in government and the nuclear industry [1]. During the decommissioning of old nuclear facilities, the facilities or sites shall be safely removed from service, and the residual radioactivity shall be reduced to the allowable range. Decommissioning involves the dismantling and decontamination of

related facilities and components, as well as the disposal and restoration of other wastes and contaminated areas. Dismantling is defined as the removal of equipment or structures for disposal or other processing. It entails choosing suitable techniques in the work scope and removal methods of equipment or structures.

At present, most of the major nuclear power plants to be decommissioned use pressurized water reactors (PWR). The main components of the primary circuit in nuclear power plants using PWR include reactor pressure vessels, coolant pumps, steam generators, etc. The dismantlement technology of nuclear reactors after the nuclear reactor

The associate editor coordinating the review of this manuscript and approving it for publication was Yangmin Li^{ID}.

shutdown is an urgent problem to be solved. However, these systems and components have a high dose of residual radioactivity and temperature, together with the large volume and quality of the related equipment and the complex shape, which make it impossible to use the conventional disassembly process. Therefore, remote-controlled manipulator technology has been an important topic to cut and handle equipment and structures of decommissioned nuclear power plants [2], [3], [4].

In this complex working environment, the decommissioned reactor is cut and disassembled using the multi-degree-of-freedom robot manipulator. Accurate trajectory tracking control is required when cutting the reactor vessel internal (RVI). However, there are many non-linear and coupling terms in the dynamics of a multi-degree-of-freedom robot manipulator. Because of its complex structure, it is difficult to obtain its dynamic model accurately. Therefore, there are many modeling errors and unmodeled parts in the dynamic model of a robot. Different end-effectors (i.e., laser cutters or plasma cutters, etc.) are used when cutting RVI with robots, which results in changes in load conditions. And due to the uncertainty of the environment of the abandoned reactor, it will cause external disturbance [5].

By estimating and compensating for the perturbation of the system, the robustness of the system can be increased, and over-conservative control gains in traditional SMC can be reduced to improve the chattering in the control input. The consolidation of the sliding perturbation observer (SPO) into the SMC (SMCSPO) demonstrates excellent trajectory-tracking performance [6]. In the traditional linear sliding mode control (LSMC), a linear sliding surface is usually used. The asymptotic convergence speed can be determined by adjusting the parameters of the sliding hyperplane, but the state error will not converge to zero in a finite time [7], [10]. In the terminal sliding mode control (TSMC), the nonlinear terminal sliding surface is introduced instead of a linear sliding surface to improve the error convergence performance of the system [8], [9].

However, in SMCSPO and TSMCSPO, the control gain can affect the observation and control performance, so the selection of optimal parameters is an important issue. In some cases, setting some parameters to a larger value will result in faster convergence speed, but it may also cause oscillation, or even reduce the stability of the system, while too small control parameters will lead to reduced convergence and observation performance. On the other hand, it is difficult to select a fixed optimal parameter due to the control system's state change and environmental interference. Therefore, it is necessary to tune the controller parameters in real time according to the state change of the system. Due to the complexity and nonlinearity of the control system, it is difficult to use a simple method to tune the parameters of the controller. However, through technicians' understanding of the characteristics of relevant controllers and their own experience, a fuzzy logic system can be designed to tune the control parameters in real-time to achieve

high-level control and improve the performance of the control system.

The results of simulation and experiments show that the fuzzy TSMCSPO algorithm has better trajectory tracking performance than the existing TSMCSPO algorithm for the robot manipulator used for nuclear reactor disassembly.

II. DISCUSSION ON CONTROL ALGORITHMS

The sliding perturbation observer (SPO) for the estimation of the system states and the perturbation will be introduced first, and then the SMCSPO integrating the SPO with the sliding mode control is illustrated. Finally, a modified TSMCSPO with a nonlinear terminal sliding mode surface, based on the conventional SMCSPO, will be introduced.

A. SLIDING PERTURBATION OBSERVER

The SPO can be used to estimate the system perturbation [6], and it has good robustness.

The state-space of a general second-order system dynamics with n-DOF can be represented as:

$$\begin{aligned}\dot{x}_{1j} &= x_{2j} \\ \dot{x}_{2j} &= f_j(\mathbf{x}) + \Delta f_j(\mathbf{x}) + \sum_{i=1}^n [b_{ji}(\mathbf{x}) u_j + \Delta b_{ji}(\mathbf{x}) u_j] + d_j(t) \\ j &= 1, \dots, n\end{aligned}\quad (1)$$

where $\mathbf{x}[\mathbf{X}_1 \dots \mathbf{X}_n]^T$ is the state vector and $\mathbf{X}_1[x_j; \dot{x}_j]^T$. The components $f_j(\mathbf{x}) \in \mathbb{R}^{n \times n}$ correspond to the nonlinear driving terms and $\Delta f_j(\mathbf{x})$ is their uncertainties. And the terms $b_{ji} \in \mathbb{R}^{n \times n}$ represent the elements of the control gain matrix and Δb_{ji} is their uncertainties, $u_j \in \mathbb{R}^{n \times 1}$ is the control input. The term $d_j \in \mathbb{R}^{n \times 1}$ is the external disturbance.

The perturbation is defined as the combination of all the uncertainties and disturbances:

$$\Psi_j(\mathbf{x}, t) = \Delta f_j(\mathbf{x}) + \sum_{i=1}^n [\Delta b_{ji}(\mathbf{x}) u_i] + d_j(t) \quad (2)$$

thus, transform (1) the form of system dynamics into (3).

$$\begin{aligned}\dot{x}_{1j} &= x_{2j} \\ \dot{x}_{2j} &= f_j(\mathbf{x}) + \sum_{j=1}^n b_j(\mathbf{x}) u_j + \Psi_j(\mathbf{x}, t).\end{aligned}\quad (3)$$

A new equivalent control input is defined as:

$$\alpha_{3j} \bar{u}_j = f_j(\mathbf{x}) + \sum_{j=1}^n b_j(\mathbf{x}) u_j \quad (4)$$

where α_{3j} is an arbitrary positive number and \bar{u}_j is new equivalent control variable, which will be detailed in the following sections. A new state variable x_{3j} is defined as:

$$x_{3j} = \alpha_{3j} x_{2j} - \Psi_j / \alpha_{3j} \quad (5)$$

where the gain α_{3j} is usually chosen as high gain for the derivative of x_{3j} to minimize the effect of the derivative of perturbation Ψ_j [6]. If the new state variable x_{3j} is estimated, Ψ_j can be consequently calculated using this relation from (5) instead of estimating it directly. The structure of SPO with the

j -th degree of freedom is as follows [3]:

$$\begin{aligned}\hat{x}_{1j} &= \hat{x}_{2j} - k_{1j} \text{sat}(\tilde{x}_{1j}) - \alpha_{1j} \tilde{x}_{1j} \\ \hat{x}_{2j} &= \alpha_{3j} \bar{u}_j - k_{2j} \text{sat}(\tilde{x}_{1j}) - \alpha_{2j} \tilde{x}_{1j} + \hat{\Psi}_j \\ \hat{x}_{3j} &= \alpha_{3j}^2 (-\hat{x}_{3j} + \alpha_{3j} \hat{x}_{2j} + \bar{u}_j) \\ \hat{\Psi}_j &= \alpha_{3j} (-\hat{x}_{3j} + \alpha_{3j} \hat{x}_{2j})\end{aligned}\quad (6)$$

where “ \wedge ” symbolizes the estimated quantity, “ \sim ” represents the error between the observed value and the actual value, i.e. $\tilde{x}_{1j} = \hat{x}_{1j} - x_{1j}$, and $\alpha_{1j}, \alpha_{2j}, k_{1j}, k_{2j}$ are positive numbers.

B. SLIDING MODE CONTROL WITH SLIDING PERTURBATION OBSERVER

SMCSPO is a combination of SPO and SMC. The estimated perturbation in SPO is applied to compensate for uncertainties and disturbances by considering the control input design.

An estimated sliding function is defined as:

$$\hat{s}_j = \hat{e}_j + c_{1j} \hat{e}_j \quad (7)$$

where $\hat{e}_j = \hat{x}_{1j} - \dot{x}_{1dj}$ is the estimated velocity tracking error, and parameters of sliding surface $c_{1j} > 0$.

The control \bar{u}_j enforces $\hat{s}_j \dot{\hat{s}}_j < 0$ outside a prescribed manifold. The desired \hat{s}_j -dynamics is selected as:

$$\dot{\hat{s}}_j = -K_j \text{sat}(\hat{s}_j) \quad (8)$$

where saturation function is defined as:

$$\text{sat}(\hat{s}_j) = \begin{cases} \hat{s}_j / |\hat{s}_j|, & \text{if } |\hat{s}_j| \geq \epsilon_{cj} \\ \hat{s}_j / \epsilon_{cj}, & \text{if } |\hat{s}_j| \leq \epsilon_{cj} \end{cases} \quad (9)$$

and where ϵ_{cj} is boundary layer of the SMC.

Using (6) and (7), the sliding surface is selected as:

$$\hat{s}_j = \hat{x}_{2j} - \frac{k_1}{\epsilon_{0j}} \tilde{x}_{1j} - \dot{x}_{1dj} + c_{1j} (\hat{x}_{1j} - x_{1dj}) \quad (10)$$

where ϵ_{0j} is boundary layer of the SPO.

According to the structure of the sliding perturbation observer in (6), the time derivative of \hat{x}_{2j} is given:

$$\dot{\hat{x}}_{2j} = \alpha_{3j} \bar{u}_j - k_{2j} \text{sat}(\tilde{x}_{1j}) - \alpha_{2j} \tilde{x}_{1j} + \hat{\Psi}_j. \quad (11)$$

Then, the derivative of the sliding function in (10) is:

$$\begin{aligned}\dot{\hat{s}}_j &= -K_j \text{sat}(\hat{s}_j) = \alpha_{3j} \bar{u}_j - \left[\frac{k_{2j}}{\epsilon_{0j}} + c_{j1} \left(\frac{k_{1j}}{\epsilon_{0j}} \right) - \left(\frac{k_{1j}}{\epsilon_{0j}} \right)^2 \right] \tilde{x}_{1j} \\ &\quad - \left(\frac{k_{1j}}{\epsilon_{0j}} \right) \tilde{x}_{2j} + c_{j1} (\hat{x}_{2j} - \dot{x}_{1dj}) - \ddot{x}_{1dj} + \hat{\Psi}_j\end{aligned}\quad (12)$$

using Eqs. (4), (8), and (12), the control law is selected as:

$$\begin{aligned}\hat{s}_j &= \frac{1}{\alpha_{3j}} - K_j \text{sat}(\hat{s}_j) + \left[\frac{k_{2j}}{\epsilon_{0j}} + c_{j1} \frac{k_{1j}}{\epsilon_{0j}} - \left(\frac{k_{1j}}{\epsilon_{0j}} \right)^2 \right] \tilde{x}_{1j} \\ &\quad + \ddot{x}_{1dj} - c_{j1} (\hat{x}_{2j} - \dot{x}_{1dj}) - \hat{\Psi}_j.\end{aligned}\quad (13)$$

The resulting \hat{s}_j -dynamics including the effects of \tilde{x}_{2j} , becomes:

$$\dot{\hat{s}}_j = -K_j \text{sat}(\hat{s}_j) - (k_{1j} / \epsilon_{0j}) \tilde{x}_{2j}. \quad (14)$$

To satisfy $\dot{\hat{s}}_j \hat{s}_j < 0$ outside the manifold $|\hat{s}_j| \geq \epsilon_{cj}$, for ensure system robustness, the gain should be selected as $K_j \geq k_{1j}^2 / \epsilon_{0j}$. Determine the K_j in outside the manifold can be given as:

$$K_j \geq (k_{1j} / \epsilon_{0j}) \Gamma_j R_{maxj} \quad (15)$$

where Γ_j is the anticipated boundary of perturbation and R_{maxj} represents the maximum ratio between \tilde{x}_{2j} and perturbation Ψ_j on some frequency.

C. TERMINAL SLIDING MODE CONTROL WITH SLIDING PERTURBATION OBSERVER

In the TSMCSPO (Terminal Sliding Mode Control with Sliding Perturbation Observer), a new form of the terminal sliding surface is applied to SPO to improve the observation and convergence performance of the existing SMCSPO and further effectively reduce the error between the estimated value and the expected value of the system state.

For the second-order system (3), a traditional terminal sliding mode on the j -th hypersurface is expressed as [8]:

$$s_j = \dot{e}_j + \beta_j e_j^{q/p}, \quad q < p \leq 2q \quad (16)$$

where p and q all are odd numbers and $\beta_j > 0$.

In contrast, an improved new form of TSMC is defined as [9]:

$$s_j = \dot{e}_j + \beta_j |e_j|^\gamma \text{sign}(e_j) \quad (17)$$

where $\text{sign}(e_j)$ is a sign function of e_j , and the interval of power γ is (0, 1). Consider (7) and (17), the new form of terminal sliding surface is applied to SPO define the estimated sliding surface as:

$$\hat{s}_j = \hat{e}_j + \beta_j |\hat{e}_j|^\gamma \text{sign}(\hat{e}_j) \quad (18)$$

where the \hat{e}_j is the same as the definition in the SMCSPO section, which is the error between the estimated and expected values of the system state for each joint of the manipulator.

Using (6) and (18) can be obtained:

$$\begin{aligned}\dot{\hat{s}}_j &= \alpha_{3j} \bar{u}_j - \left[\frac{k_{2j}}{\epsilon_{0j}} - \left(\frac{k_1}{\epsilon_{0j}} \right)^2 \right] \tilde{x}_{1j} - \left(\frac{k_1}{\epsilon_{0j}} \right) \tilde{x}_{2j} \\ &\quad - \dot{x}_{1dj} + \beta_j \gamma |\hat{e}_j|^{\gamma-1} \dot{\hat{e}}_j + \hat{\Psi}_j.\end{aligned}\quad (19)$$

A sliding dynamic can be expressed as:

$$s_j = -\eta_{1j} \text{sign}(s_j) - \eta_{2j} |s_j|^r \text{sign}(s_j) \quad (20)$$

where parameter η_{1j} and η_{2j} are positive numbers, and η_{1j} should be greater than the perturbation boundary of the system. Therefore, considering (15), the sliding dynamics can be represented as:

$$\dot{\hat{s}}_j = -\Gamma_j R_{maxj} \left(\frac{k_1}{\epsilon_{0j}} \right) \text{sign}(\hat{s}_j) - \eta_{2j} |\hat{s}_j|^r \text{sign}(\hat{s}_j) - \left(\frac{k_1}{\epsilon_{0j}} \right) \tilde{x}_{2j} \quad (21)$$

and the Lyapunov description of TSMCSPO can be shown as:

$$\begin{aligned} \dot{V} &= \hat{s}_j \hat{s}_j \\ &= \hat{s}_j \left(-\Gamma_j R_{maxj} \text{sign}(s_j) - \eta_{2j} |e_j|^r \text{sign}(s_j) - \left(\frac{k_1}{\epsilon_{oj}} \right) \tilde{x}_{2j} \right) \\ &\leq \eta_{2j} 2^{\frac{r+1}{2}} V^{\frac{r+1}{2}} \leq 0. \end{aligned} \quad (22)$$

Then, using (4), (19), and (21), the new control law is selected as:

$$\begin{aligned} \bar{u}_j &= \frac{1}{\alpha_{3j}} \left\{ -\Gamma_j R_{maxj} \text{sign}(\hat{s}_j) - \eta_{2j} |e_j|^r \text{sign}(s_j) \right. \\ &\quad + \left[\frac{k_{2j}}{\epsilon_{oj}} - \left(\frac{k_{1j}}{\epsilon_{oj}} \right)^2 \right] \tilde{x}_{1j} + \ddot{x}_{1dj} - \hat{\Psi}_j \\ &\quad \left. - \beta_j \gamma |\hat{e}_j|^{\gamma-1} \left(\hat{x}_{2j} - \left(\frac{k_{1j}}{\epsilon_{oj}} \right) \tilde{x}_{1j} - \dot{x}_{1dj} \right) \right\}. \end{aligned} \quad (23)$$

To avoid the singularity problem following must be satisfied:

$$\frac{d}{dt} (|e_j|^\gamma) = \begin{cases} \gamma |\dot{e}_j|^{\gamma-1} \dot{e}_j, & \text{if } \dot{e}_j \neq 0, e \neq 0 \\ \gamma |\Delta|^{\gamma-1} \dot{e}_j, & \text{if } \dot{e}_j \neq 0, e = 0 \\ 0, & \text{if } \dot{e}_j = 0, e = 0 \end{cases} \quad (24)$$

where $\Delta > 0$ is a small positive number close to zero.

III. CONTROLLER DESIGN

In this chapter, first, a general approach to configuring the parameters of SMCSPO and TSMCSPO will be presented in the first section, and the mechanisms underlying the effects of these parameters on control performance will be illustrated. Based on this, the fuzzy TSMCSPO proposed in this study will then be introduced.

A. CONTROLLER PARAMETER DESIGN PROCEDURE

This section presents the general design procedure of parameters of SMCSPO and TSMCSPO for a system while considering the system characteristic and hardware limitations [9].

When the condition $|\tilde{x}_{1j}| < \epsilon_{oj}$ and $\hat{s}_j < \epsilon_{cj}$ are achieved, i.e., the double sliding is in effect, observer and s_j dynamics take the form:

$$\begin{aligned} &\begin{bmatrix} \dot{\tilde{x}}_{1j} \\ \dot{\tilde{x}}_{2j} \\ \dot{\tilde{x}}_{3j} \\ \dot{s}_j \end{bmatrix} \\ &= \begin{bmatrix} -\frac{k_{1j}}{\epsilon_{oj}} & 1 & 0 & 0 \\ -\frac{k_{2j}}{\epsilon_{oj}} & \alpha_{3j}^3 & -\alpha_{3j} & 0 \\ 0 & \alpha_{3j}^3 & -\alpha_{3j}^2 & 0 \\ \frac{k_{2j}}{\epsilon_{oj}} - (c - \frac{k_{1j}}{\epsilon_{oj}})^2 & -(2c + \alpha_{3j}^2) & \alpha_{3j} & -c \end{bmatrix} \\ &\times \begin{bmatrix} \tilde{x}_{1j} \\ \tilde{x}_{2j} \\ \tilde{x}_{3j} \\ s_j \end{bmatrix} + \begin{bmatrix} 0 \\ 0 \\ 0 \\ 1 \end{bmatrix} \frac{\dot{\Psi}}{\alpha_{3j}}. \end{aligned} \quad (25)$$

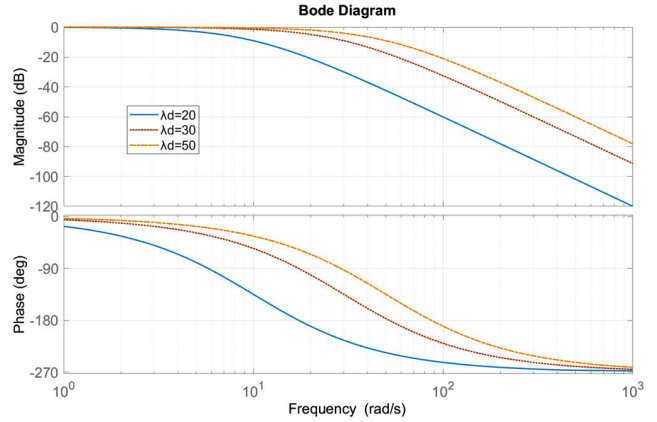


FIGURE 1. Bode diagram between estimated perturbation and actual perturbation of the system.

According to the observer and s_j dynamics, the associated characteristic equation is:

$$[\lambda + c_{j1}] \left[\lambda^3 + \left(\frac{k_{1j}}{\epsilon_{oj}} \right) \lambda^2 + \left(\frac{k_{2j}}{\epsilon_{oj}} \right) \lambda + \alpha_{3j}^2 \left(\frac{k_{2j}}{\epsilon_{oj}} \right) \right] = 0. \quad (26)$$

The desired characteristic equation and desired eigenvalue λ_d can be designed by pole assignment method. Desired characteristic equation can be: $p(\lambda_d) = (\lambda + \lambda_d)^4$, then design the controller by selecting λ_d .

This leads to the following design solutions:

$$\frac{k_{1j}}{\epsilon_{oj}} = 3\lambda_d, \quad \frac{k_{2j}}{k_{1j}} = \lambda_d, \quad \alpha_{3j} = \sqrt{\frac{\lambda_d}{3}}, \quad c = \frac{K_j}{\epsilon_{oj}} = \lambda_d. \quad (27)$$

The λ_d determines the cut-off frequency of the lowpass filter between the Ψ_j with $\hat{\Psi}_j$ [5]. The frequency domain relation between perturbation estimation value $\hat{\Psi}(p)$ and actual perturbation of system $\Psi(p)$ can be obtained as:

$$\frac{\hat{\Psi}(p)}{\Psi(p)} = \frac{\lambda_d^3}{(p + \lambda_d)^3}. \quad (28)$$

The bode diagram of the frequency domain relation at values of different λ_d is shown in Figure 1.

Frequency domain analysis shows that if the value of λ_d is increased, the cut-off frequency will also increase, which means that the estimation performance of SPO for perturbation is improved. However, if λ_d is configured to an excessive value, it will cause oscillation problems. Therefore, it is necessary to optimize the value of λ_d , so that the system can avoid oscillation problems while having good perturbation estimation accuracy.

The frequency domain relation between velocity estimation error \tilde{x}_2 and perturbation estimation error $\tilde{\Psi}(p)$ can be obtained as:

$$\frac{\tilde{x}_2(p)}{\tilde{\Psi}(p)} = \frac{1}{s + \lambda_d}. \quad (29)$$

The bode diagram of the frequency domain relation at value of different λ_d is shown in Figure 2.

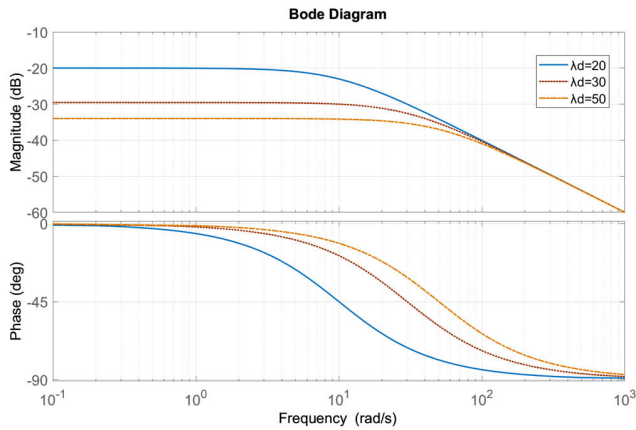


FIGURE 2. Bode Diagram between velocity estimation error and perturbation estimation error.

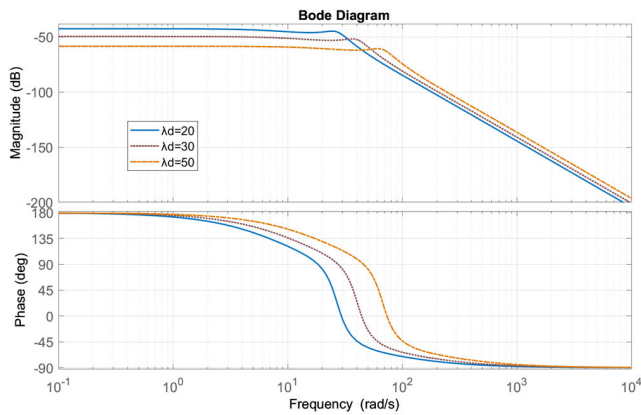


FIGURE 3. Bode Diagram between velocity estimation error and perturbation estimation error.

In SPO, tuning parameter of λ_d according to the estimation error Ψ through fuzzy logic, to obtain a better estimation effect on the perturbed $\tilde{\Psi}$.

However, in the actual hardware system, the perturbation estimation error $\tilde{\Psi}$ cannot be known. Because the perturbation in the real physical system contains such random elements as an environmental disturbance. Therefore, it is necessary to find other variables that are both positively correlated with the perturbation estimation error and can be observed, such as the estimated value of the position tracking error \hat{e} . By inducing the previous formula, the transfer function between \hat{e} and $\tilde{\Psi}$ can be obtained as follows:

$$\frac{\hat{e}(p)}{\tilde{\Psi}(p)} = \frac{-3\lambda_d p - 9\lambda_d^2}{p^4 + 5\lambda_d p^3 + 6\lambda_d^2 p^2 + 9\lambda_d^3 p + 4\lambda_d^4}. \quad (30)$$

The Bode Diagram of the frequency domain relation at values of different λ_d is shown in Figure 3.

In addition, the value of parameter λ_d is also limited by the characteristics of the actual hardware system [6], i.e., sampling frequency, measurement delay, etc. Once $|\tilde{x}_{1j}| < \epsilon_{oj}$

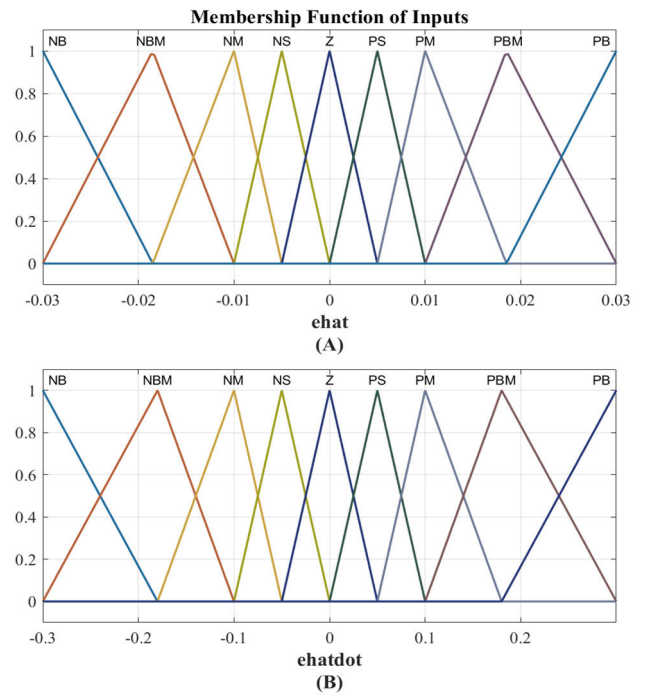


FIGURE 4. Membership function of fuzzy system input: (A) \hat{e} and (B) $\dot{\hat{e}}$.

the observer sliding mode dynamics become:

$$\dot{\tilde{x}}_{1j} + \frac{k_{1j}}{\epsilon_{oj}} \tilde{x}_{1j} = \tilde{x}_{2j}. \quad (31)$$

Consider τ^{hw} to be the dominant time delay in the hardware, the breaking point of the sliding function dynamics inside a manifold cannot exceed [12]:

$$\lambda_d \leq \frac{1}{5\tau^{hw}}. \quad (32)$$

When the tuning parameter λ_d of the fuzzy system is used, the tuning range shall not exceed this limit to ensure stability.

For the TSMCSPO, it can be found that if the parameter η_2 is larger, the convergence time will be reduced, but also because the slope of the middle sliding surface in (21) is steeper, it will lead to more chattering [8]. Therefore, in this study, the fuzzy logic system will also be used to tune parameter η_2 in real time to improve these problems. The detailed process of real-time tuning of these two parameters will be described in the next section.

B. DESIGN OF FUZZY TERMINAL SMC WITH SPO ALGORITHM

According to the description of the controller design process in the previous section and the analysis of the influence mechanism of the relevant parameters on the control performance, as shown in Figure 4, the fuzzy logic system is designed to tune the parameters λ_d and η_2 in real-time according to the estimated system state variables.

The membership function of the designed fuzzy system input is shown in Figure 4, where (A) is the membership

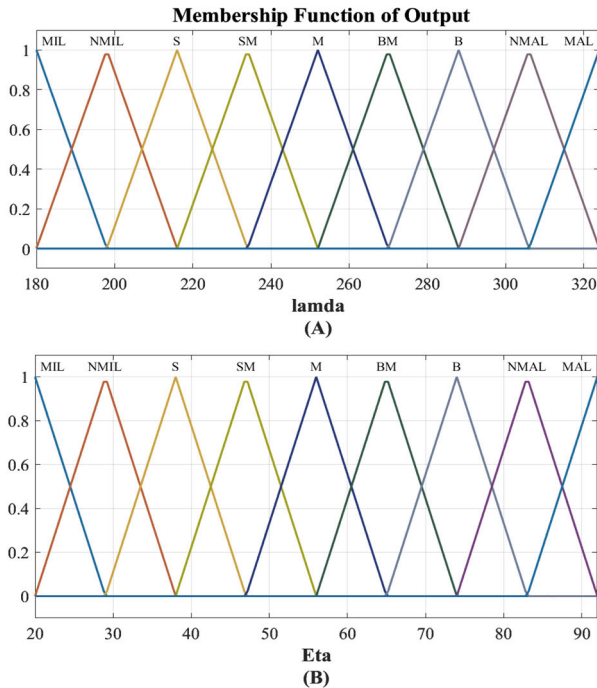


FIGURE 5. Membership function of fuzzy system output: (A) λ_d and (B) η_2 .

function of error estimation \hat{e} , and (B) is the membership function of speed estimation error \hat{e} .

As shown in Figure 4, there are 9 fuzzy sets for both inputs, where ‘NB’ means ‘Negative Big’, ‘NM’ means ‘Negative Medium’, ‘NBM’ means ‘Negative Big Medium’, ‘NS’ means ‘Negative Small’, ‘Z’ represents ‘Zero’, ‘PS’ means ‘Positive Small’, ‘PM’ means ‘Positive Medium’, ‘PBM’ represents ‘Positive Big Medium’ and ‘PB’ represents ‘Positive Big’.

In the fuzzy set of λ_d , The consideration interval is (180, 322.6), i.e., the λ_d will change in real-time within this interval. Whereas for η_2 the interval was (20, 91.5).

The sampling time of the simulation system and the hardware experimental system is 0.3(ms) and 1.0(ms) respectively (This will be mentioned in the next chapter). Therefore, in the simulation and hardware experiments, it is safe to set the limits of $\lambda_d < 666.7$ and $\lambda_d < 200.0$ respectively. In this study, when using the real-time tuning parameters of the fuzzy system, the value intervals of λ_d are respectively (180, 322.6) and (20, 100), both within their respective limits. Therefore, in this study, although the controller parameters are tuned in real-time according to the system state through the fuzzy logic system, the control system can be concluded to be stable because the relevant parameters are always within the limits.

As shown in Figure 5, there are 9 fuzzy sets for parameters λ_d and η_2 respectively. Where ‘MIL’ means ‘Minimum Limit’, ‘NMIL’ means ‘Near Minimum Limit’, ‘S’ means ‘Small’, ‘SM’ means ‘Small Medium’, ‘M’ represents ‘Medium’, ‘BM’ means ‘Big Medium’, ‘B’ means ‘Big’,

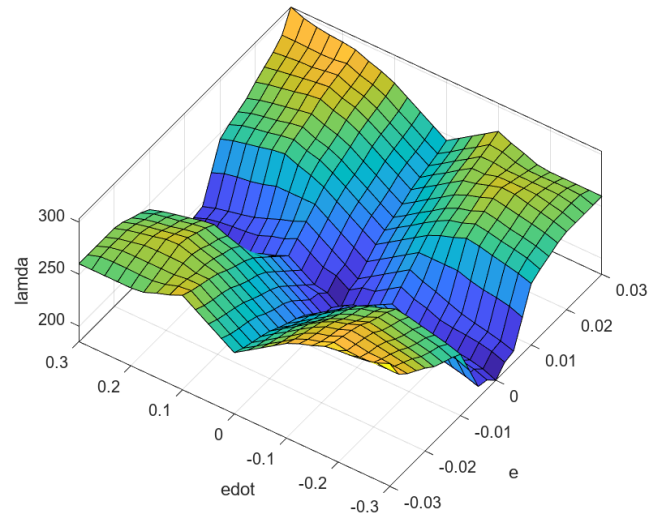


FIGURE 6. According to the output (λ_d) surface of the fuzzy logic system.

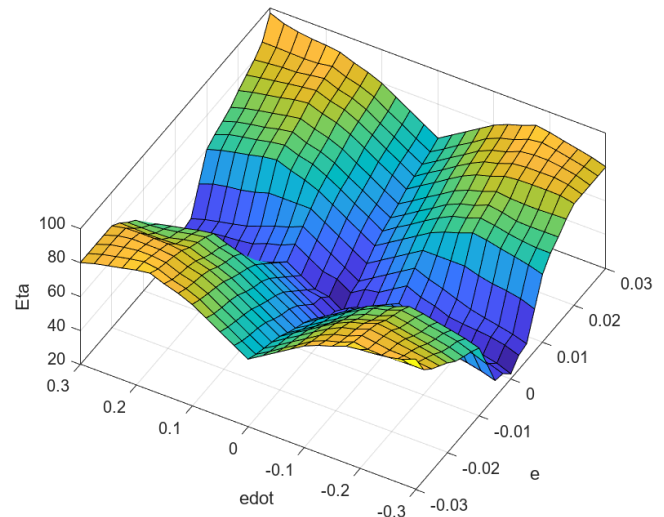


FIGURE 7. According to the output (η_2) surface of fuzzy logic system.

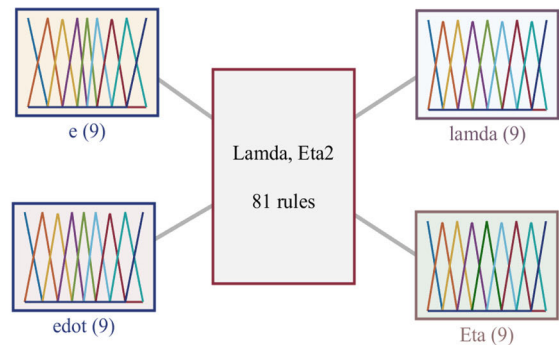


FIGURE 8. The fuzzy system with 81 fuzzy rules.

‘NMAL’ represents ‘Near Maximum Limit’ and ‘MAL’ represents ‘Maximum Limit’.

The output surface of the fuzzy system with two parameters is shown in Figures 6 and 7 respectively.

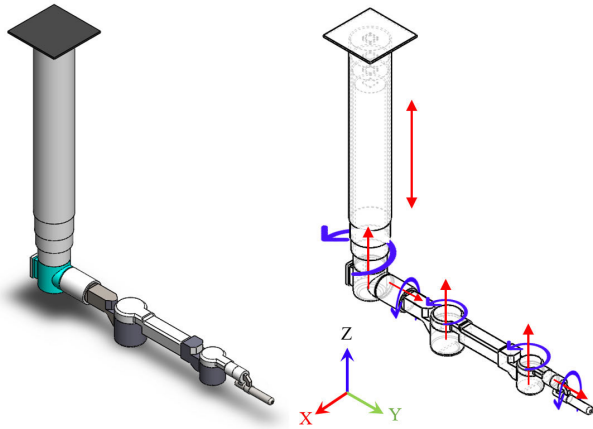


FIGURE 9. Model view and axis configuration of the reactor dismantlement robot.

The fuzzy logic system was designed as follows, which altogether contains 81 fuzzy rules due to a total of 2 inputs corresponding to 9 fuzzy sets, respectively. The fuzzy rules and fuzzy system output are illustrated with the following 3 examples:

If \hat{e} is Zero and $\dot{\hat{e}}$ is Zero, Then λ_d is Minimum Limit and η_2 is Minimum Limit.

If \hat{e} is Positive Big and $\dot{\hat{e}}$ is Zero, Then λ_d is Small Medium and η_2 is Small Medium.

If \hat{e} is Positive Big and $\dot{\hat{e}}$ is Positive Big, Then λ_d is Limit and η_2 is Limit.

IV. SYSTEM AND EXPERIMENTAL PLATFORM

This chapter presents the existing system configuration, design, robot manipulator model, and the current study’s experimental setup. The overall system consists of a 2-DOF crane system, and a 6-DOF SCARA-type robot (1-DOF prismatic telescope and 5-DOF robot arm). In this study, the robot manipulator with 5 rotary joints is mainly considered. In addition, the simulation system also includes the PWR model with cutting. The robot manipulator will work in the underwater environment inside the PWR, so the underwater dynamics of the robot manipulator are also considered.

A. DYNAMICS OF THE NUCLEAR REACTOR DECOMMISSIONING ROBOT MANIPULATOR

The model view of the reactor dismantlement robot manipulator is shown in Figure 9, it has a total of (5+1) degrees of freedom, including five revolute joints and one additional telescopic prismatic joint. Table 1 lists the mass, inertia, and damping of the link for revolute joints.

B. SIMULATION ENVIRONMENT

Figure 10 presents the Simulink model of the virtual system, i.e., crane, dismantlement robot manipulator, and the RVI, which consists of using the SimMechanics toolbox. In MATLAB/Simulink, the disassembly of a

TABLE 1. Information on the reactor dismantlement robot.

Link	Mass (kg)	Link Lengths (m)	Inertia (N · m)	Damper (N · s/m)
1	88	0.340	30.6	8.57
2	139.7	0.410	0.77	2.72
3	129.4	0.817	3.40	1.42
4	20.8	0.361	0.15	0.6
5	11.7	0.365	0.15	1.5

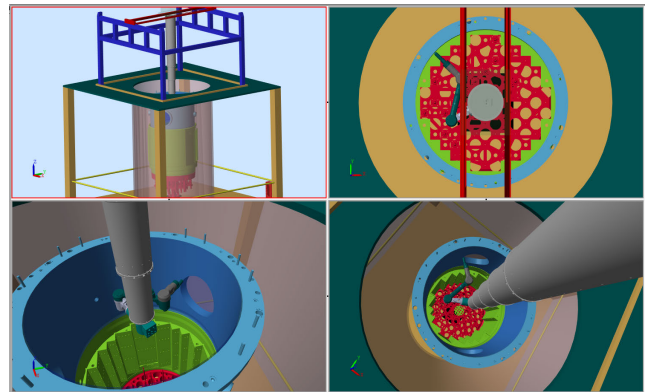


FIGURE 10. Nuclear reactor dismantlement virtual simulation in MATLAB.

decommissioned nuclear reactor is simulated using this robot manipulator model.

C. EXPERIMENTAL SETUP

In this study, although the cutting process of the reactor in the reactor’s internal environment using robot manipulators was simulated in the MATLAB/Simulink environment, it is difficult to carry out experiments in the reactor’s internal environment based on the current conditions. Therefore, the Indy7 6-DOF robot produced by Neuromecka Company is used as the experimental platform to alternate the 5-DOF robot manipulator for hardware experiments.

In this study, for the hardware experimental platform, 5 degrees of freedom are considered and based on this, the control performance is analyzed. Figure 11 shows the robot manipulator experimental platform.

In the hardware experiment, the sampling frequency of the system is set to 1000 Hz. In this study, the signal compression method (SCM) is used to identify each link of the robot manipulator system [21]. The linear dynamic parameters of each link of the system estimated by this method are shown in Table 2, and the uncertainties and nonlinear terms of the system will be considered perturbations.

V. RESULT OF SIMULATION AND EXPERIMENT

In this chapter, the results of these simulations and experiments are analyzed and illustrated. The simulation and



FIGURE 11. Indy7 6-DOF robot experimental platform.

TABLE 2. Indy 7 robot manipulator link information.

Link	Inertia($N \cdot m$)	Damper($N \cdot s/m$)
1	6.3915	104.0536
2	26.7698	153.6587
3	5.9453	48.2559
4	1.8262	18.9189
5	1.6023	5.0633
6	0.9383	5.4795

experimental results show that the new algorithm has superior control performance.

A. RESULT OF SIMULATION FOR TRAJECTORY TRACKING

The simulation is performed in MATLAB/Simulink. The desired trajectory of each joint of the reactor decommissioning robot manipulator in the simulation is shown in Figure 12, and the corresponding desired velocity is shown in Figure 13.

First, in TSMCSPO, the parameters λ_d and η_2 are set as large constants as follows:

$$\lambda_d = [230, 240, 260, 250, 220], \quad \eta_2 = [65, 70, 75, 70, 60]$$

the results of the trajectory tracking error of each joint of the robot manipulator are shown in Figure 14. Where, λ_d and η_2 are vectors containing five elements, and each value corresponds to each degree of freedom.

In Figure 14, the enlarged image of the part in the small grey square box is shown in Figure 15. It is shown that when λ_d is set to a larger constant value, the maximum overshoot of the error will be reduced, but oscillation will occur in each joint.

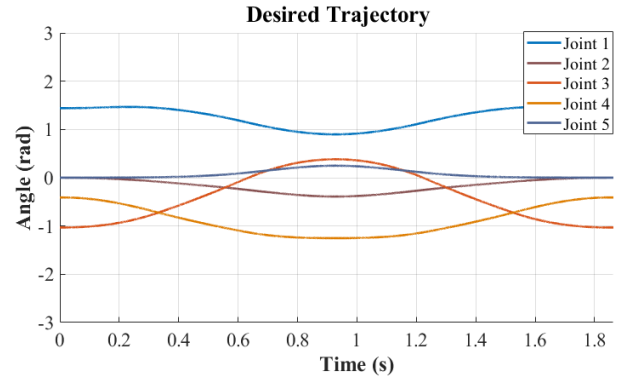


FIGURE 12. Reference trajectory for each joint.

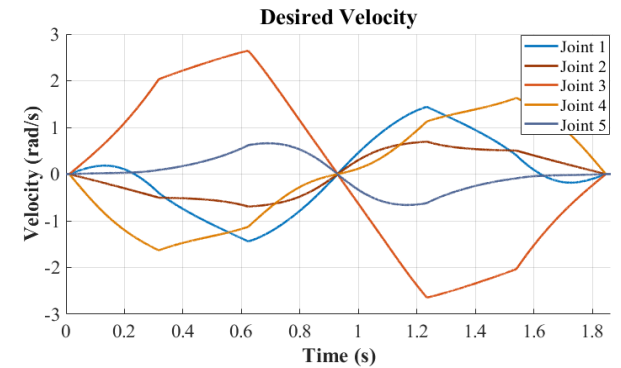


FIGURE 13. Desired velocity for each joint.

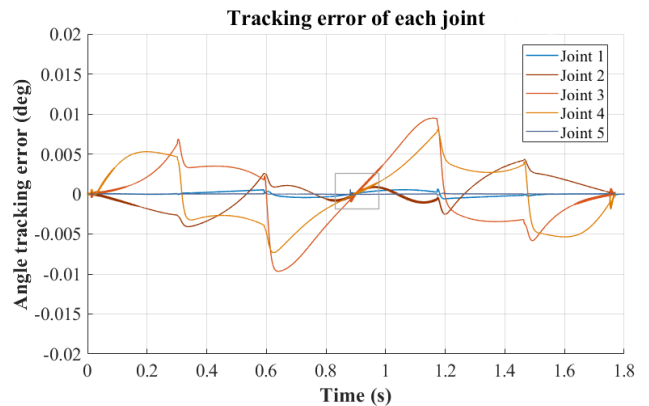


FIGURE 14. Simulation results of TSMCSPO with large parameters.

When TSMCSPO with the number of the parameters λ_d and η_2 are set as smaller constants as follows:

$$\lambda_d = [185, 190, 200, 205, 180], \quad \eta_2 = [25, 30, 35, 40, 20]$$

It can be seen from Figure 16 that when the λ_d and η_2 are set as small constants, the chattering problem is avoided, however the observation and convergence performance of the controller is damaged, resulting in a significant increase in the maximum overshoot of the trajectory tracking error.

By comparing the two simulation results, it is shown that when the parameter is set to a smaller value, the estimation

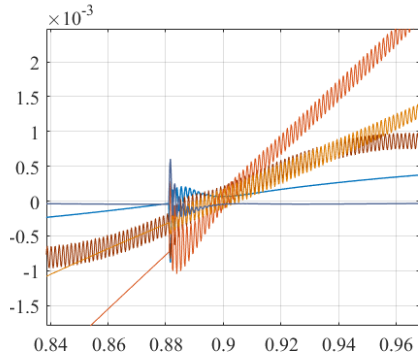


FIGURE 15. Enlarged image.

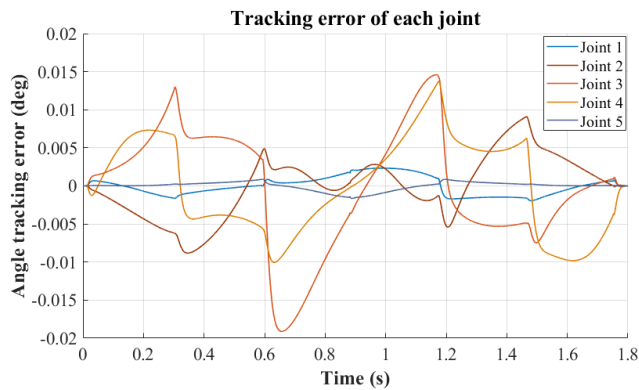


FIGURE 16. Simulation results of TSMCSPO with small parameters.

and control performance will be degraded, which will lead to a larger trajectory tracking error. When the parameter is set to a larger value, the tracking error will be reduced, and the overshoot will be significantly reduced, but chattering will occur.

Using the proposed fuzzy logic system, the system parameters tuned in real-time according to the values of \hat{e} and $\dot{\hat{e}}$ are shown in Figure 17. When using the fuzzy logic system to tune the parameters of TSMCSPO in real-time, the result of the trajectory tracking error of the system state is shown in Figure 18.

The simulation results show that when the fuzzy logic system is used to tune the parameters of TSMCSPO in real-time, the chattering phenomenon can be effectively avoided and the trajectory tracking error of the system can be reduced because the parameters are continuously adjusted to the optimum according to the system state. Therefore, the good control performance of the new algorithm is verified through simulation. In the next section, the performance of the algorithm on the hardware robot system will be analyzed through experiments.

B. RESULT OF EXPERIMENT

This section introduces the experimental results of trajectory tracking when the existing TSMCSPO algorithm and the new fuzzy TSMCSPO proposed in this research are applied

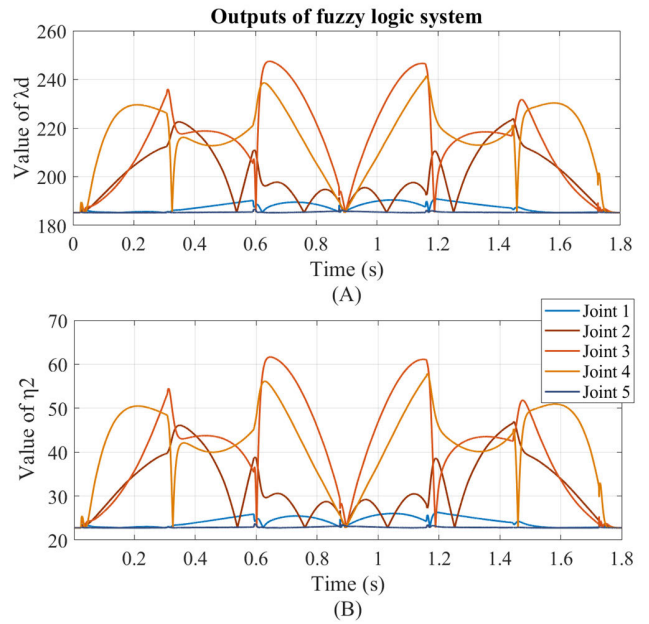


FIGURE 17. Outputs of fuzzy logic system: (A) λ_d and (B) η_2 .

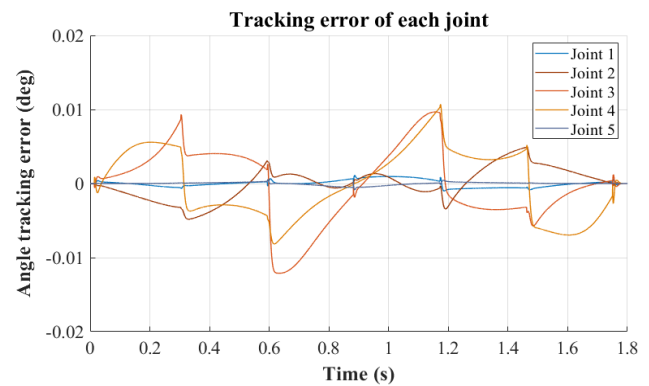


FIGURE 18. Simulation results of fuzzy TSMCSPO.

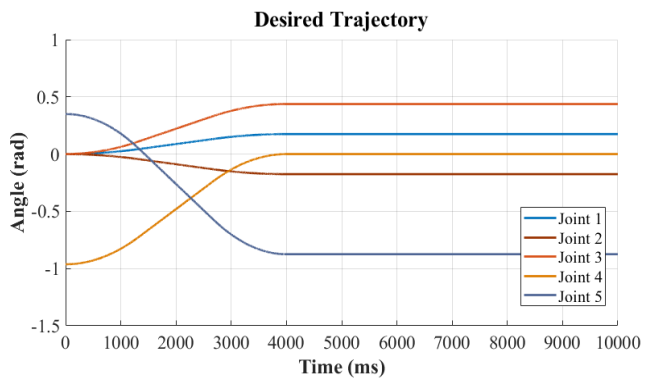


FIGURE 19. Reference trajectories in the experiment.

to the robot manipulator hardware experimental platform. The 6-DOF robot manipulator experimental platform is

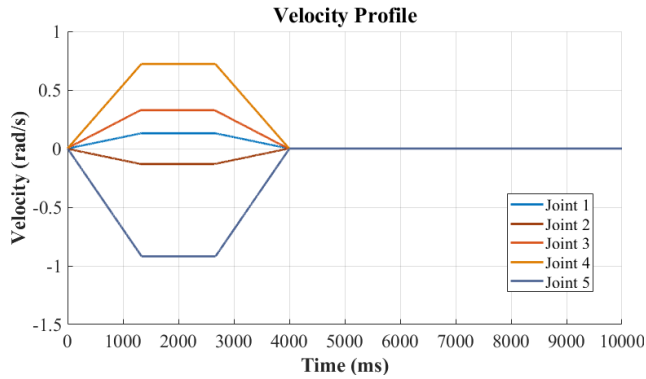


FIGURE 20. Velocity profile of the reference trajectory.

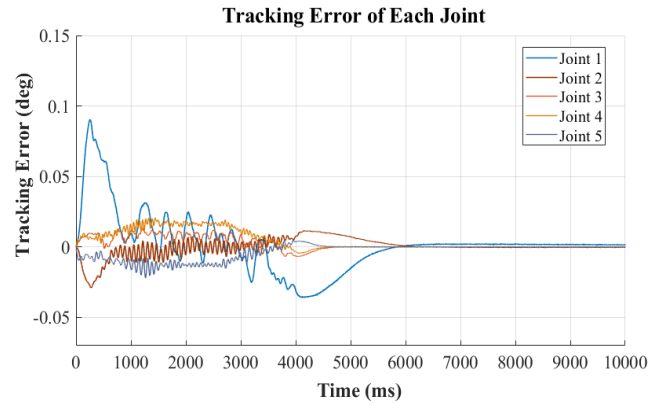


FIGURE 22. Experiment results of TSMCSPO with large parameters.

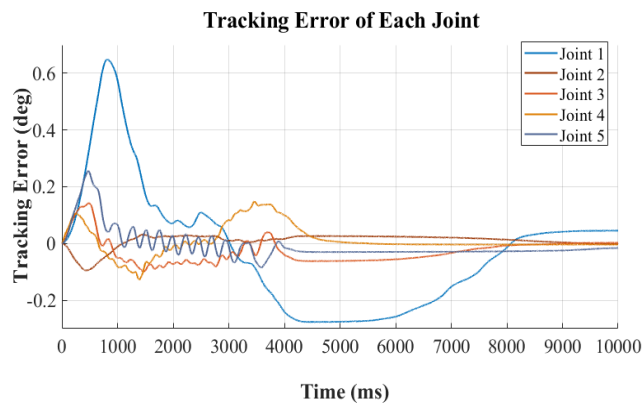


FIGURE 21. Experiment results of TSMCSPO with small parameters.

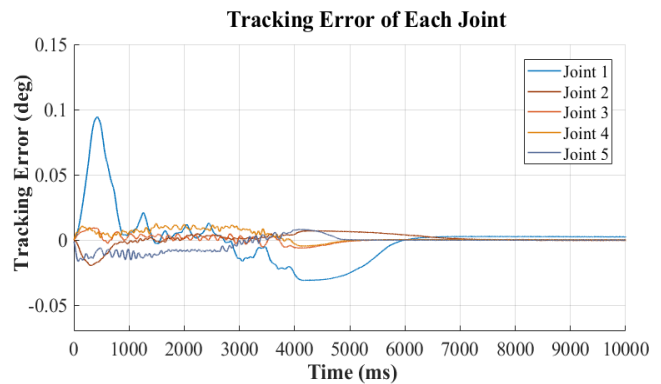


FIGURE 23. Experiment results of fuzzy TSMCSPO.

shown in Figure 11. Considering that the characteristics of the Indy7 robot manipulator platform are different from that of the 5-DOF reactor disassembly robot, the value ranges considered when tuning relevant parameters using fuzzy logic systems are slightly different, but the methods are the same. By comparing the experimental results, the control performance of the proposed algorithm on the actual hardware robot manipulator is analyzed and verified.

The reference trajectory of the robot manipulator in this experiment is shown in Figure 19, and the corresponding velocity profile is shown in Figure 20.

The corresponding experimental results of tracking error by TSMCSPO are shown in Figure 21 when the parameters are small. The selected parameters by trial and error are as follows:

$$\lambda_d = [36, 25, 36, 38, 38], \eta_2 = [21, 10, 18, 20, 20]$$

The tracking error results of each joint with large parameters are shown in Figure 22, and the corresponding parameters are as follows:

$$\lambda_d = [80, 85, 90, 95, 80], \eta_2 = [45, 36, 52, 55, 50]$$

By comparing the experimental results of TSMCSPO with different parameters λ_d , it can be seen that similar to the

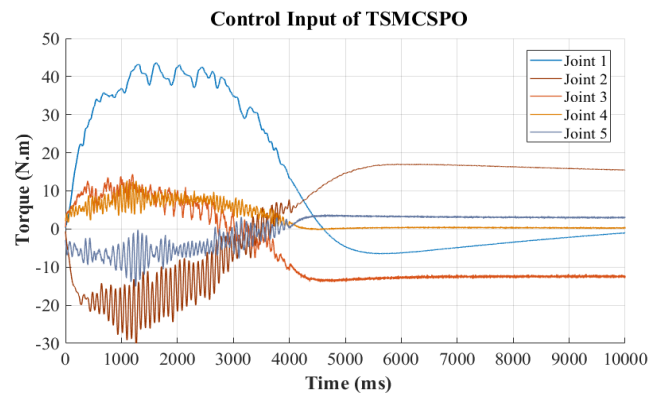


FIGURE 24. Control inputs of TSMCSPO with large constant parameters.

simulation results when using larger parameters, the error is reduced, but it will lead to oscillation, and this problem is more significant in the hardware robot manipulator experiment. Figure 23 shows the experimental results using the fuzzy TSMCSPO under the same reference trajectory. The experimental results show that fuzzy TSMCSPO effectively avoids the problems of fixed parameter TSMCSPO and has

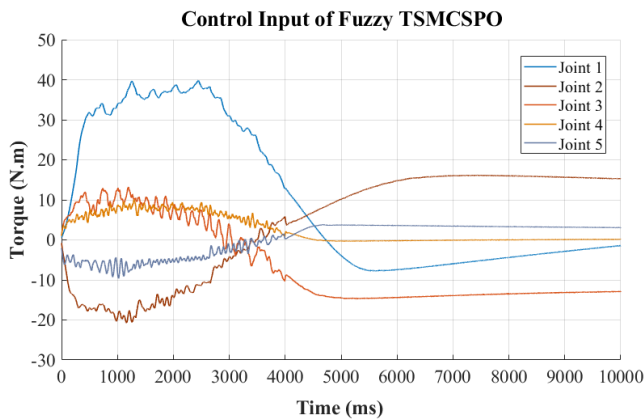


FIGURE 25. Control inputs of fuzzy TSMCSPO.

better estimation and control performance, which reduces the tracking error and avoids oscillations with large parameters.

Figure 24 shows the control input in the experiment when TSMCSPO is used with the same large parameter λ_d as shown in Figure 22, while Figure 25 corresponds to the control input when fuzzy TSMCSPO is used. By comparing the control inputs of the experiments, it is more obvious that too large parameters lead to the oscillation problem of TSMCSPO, which is effectively avoided in the proposed new fuzzy TSMCSPO.

VI. CONCLUSION

In the process of decommissioning old nuclear power plant units, multi-degree-of-freedom robot manipulators are needed to cut and disassemble nuclear reactors and related components. In the reactor environment, robot manipulators need robust control algorithms with excellent performance to achieve better trajectory tracking and compensate for uncertainties in the environment. In the existing research, SMCSPO and TSMCSPO algorithms are applied to the simulation of a reactor dismantlement robot manipulator, and the relevant research results showed that they have good control performance. However, it is known that the parameter tuning of the SMCSPO and TSMCSPO is always a key problem. Due to the control system's state change and environmental disturbance, it is difficult to select the fixed optimal parameters.

Aiming at this problem, based on TSMCSPO, a fuzzy TSMCSPO algorithm is designed by using the fuzzy logic method, which can perform real-time parameter tuning according to system state changes during robot manipulator trajectory tracking.

In this research, the simulation was carried out in Simulink and the experiment was carried out in the laboratory based on a 6-DOF robot manipulator platform. The simulation and experimental results showed that the fuzzy TSMCSPO with real-time fuzzy parameter tuning function has less tracking error and chattering than show the traditional TSMCSPO with

fixed parameters. Therefore, it is verified that the trajectory tracking control effect of the system is improved and the problems of the traditional TSMCSPO are solved.

REFERENCES

- [1] Nuclear Energy Agency, *Decommissioning of Nuclear Power Plants: Policies, Strategies, and Costs*, OECD, Paris, France, 2003.
- [2] J. M. Detriche, "Innovations in dismantling robotics," *Nucl. Eng. Des.*, vol. 182, no. 3, pp. 267–276, Jun. 1998.
- [3] I. Tsitsimpelis, C. J. Taylor, B. Lennox, and M. J. Joyce, "Evaluation methodology of a manipulator actuator for the dismantling process during nuclear decommissioning," *Prog. Nucl. Energy*, vol. 111, pp. 109–124, May 2019.
- [4] J. Park, C.-H. Kim, K.-M. Jeong, B.-S. Choi, and J. Moon, "A review of ground-based robotic systems for the characterization of nuclear environments," *Ann. Nucl. Energy*, vol. 91, pp. 22–24, Mar. 2016.
- [5] S. J. Abbasi, H. Khan, and M. C. Lee, "Trajectory tracking control of multi-DOF robot without considering system dynamics," *Int. J. Control, Autom. Syst.*, vol. 19, no. 9, pp. 2959–2970, Sep. 2021.
- [6] J. T. Moura, H. Elmali, and N. Olgac, "Sliding mode control with sliding perturbation observer," *J. Dyn. Syst., Meas., Control*, vol. 119, no. 4, pp. 657–665, Dec. 1997.
- [7] X. Yu and Z. Man, "Fast terminal sliding-mode control design for nonlinear dynamical systems," *IEEE Trans. Circuits Syst.*, vol. 49, no. 2, pp. 261–264, Feb. 2002.
- [8] J. Wang, M. C. Lee, K. D. Kallu, S. J. Abbasi, and S. Ahn, "Trajectory tracking control of a hydraulic system using TSMCSPO based on sliding perturbation observer," *Appl. Sci.*, vol. 9, no. 7, p. 1455, Apr. 2019.
- [9] M. Chen, Q.-X. Wu, and R.-X. Cui, "Terminal sliding mode tracking control for a class of SISO uncertain nonlinear systems," *ISA Trans.*, vol. 52, no. 2, pp. 198–206, Mar. 2013.
- [10] S. Yu, X. Yu, B. Shirinzadeh, and Z. Man, "Continuous finite-time control for robotic manipulators with terminal sliding mode," *Automatica*, vol. 41, no. 11, pp. 1957–1964, Nov. 2005.
- [11] L. Wang, T. Chai, and L. Zhai, "Neural-network-based terminal sliding-mode control of robotic manipulators including actuator dynamics," *IEEE Trans. Ind. Electron.*, vol. 56, no. 9, pp. 3296–3304, Sep. 2009.
- [12] J. T. Moura, R. G. Roy, and N. Olgac, "Sliding mode control with perturbation estimation (SMCPE) and frequency shaped sliding surfaces," *J. Dyn. Syst., Meas., Control*, vol. 119, no. 3, pp. 584–588, Sep. 1997.
- [13] W. Jie, Z. Yudong, B. Yulong, H. H. Kim, and M. C. Lee, "Trajectory tracking control using fractional-order terminal sliding mode control with sliding perturbation observer for a 7-DOF robot manipulator," *IEEE/ASME Trans. Mechatronics*, vol. 25, no. 4, pp. 1886–1893, Aug. 2020.
- [14] J. Zhang, F. Zhu, H. R. Karimi, and F. Wang, "Observer-based sliding mode control for T-S fuzzy descriptor systems with time delay," *IEEE Trans. Fuzzy Syst.*, vol. 27, no. 10, pp. 2009–2023, Oct. 2019.
- [15] M. R. Soltanpour, M. H. Khooban, and M. Soltani, "Robust fuzzy sliding mode control for tracking the robot manipulator in joint space and in presence of uncertainties," *Robotica*, vol. 32, no. 3, pp. 433–446, May 2014.
- [16] Y.-K. Liu, N. Chao, and A. Ayodeji, "Continuous finite-time control for robotic manipulators with terminal sliding mode," *CIRP Ann.*, vol. 38, pp. 951–966, Jan. 2018.
- [17] H. Khan, M. C. Lee, J. W. Lee, C. Li, and M. Salman, "Force/torque-based impedance control with perturbation observer—Toward high payload system robust trajectory tracking," *IEEE Access*, vol. 10, pp. 119150–119161, 2022.
- [18] M. K. Park, M. C. Lee, and W. S. Yoo, "Sliding mode control with fuzzy adaptive perturbation compensator for 6-DOF parallel manipulator," *KSME Int. J.*, vol. 18, no. 4, pp. 535–549, Apr. 2004.
- [19] Z. Chen, F. Huang, C. Yang, and B. Yao, "Adaptive fuzzy backstepping control for stable nonlinear bilateral teleoperation manipulators with enhanced transparency performance," *IEEE Trans. Ind. Electron.*, vol. 67, no. 1, pp. 746–756, Jan. 2020.
- [20] S. Ma, S. Hirose, and H. Yoshinada, "Development of a hyper-redundant multijoint manipulator for maintenance of nuclear reactors," *Adv. Robot.*, vol. 9, no. 3, pp. 281–300, Jan. 1994.
- [21] M. C. Lee and N. Aoshima, "Identification and its evaluation of the system with a nonlinear element by signal compression method," *Trans. Soc. Instrum. Control Eng.*, vol. 25, no. 7, pp. 729–736, 1989.

[22] Y. Guo and P.-Y. Woo, "An adaptive fuzzy sliding mode controller for robotic manipulators," *IEEE Trans. Syst., Man, Cybern. A, Syst. Humans*, vol. 33, no. 2, pp. 149–159, Mar. 2003.

[23] H.-H. Kim, M. C. Lee, H.-J. Cho, J.-H. Hwang, and J.-S. Won, "SMCSPO-based robust control of AUV in underwater environments including disturbances," *Appl. Sci.*, vol. 11, no. 22, p. 10978, Nov. 2021.

[24] B. K. Yoo and W. C. Ham, "Adaptive control of robot manipulator using fuzzy compensator," *IEEE Trans. Fuzzy Syst.*, vol. 8, no. 2, pp. 186–199, Apr. 2000.

[25] Q. Gao, L. Liu, G. Feng, Y. Wang, and J. Qiu, "Universal fuzzy integral sliding-mode controllers based on T-S fuzzy models," *IEEE Trans. Fuzzy Syst.*, vol. 22, no. 2, pp. 350–362, Apr. 2014.

[26] M. Van, H.-J. Kang, and K.-S. Shin, "Backstepping quasi-continuous high-order sliding mode control for a Takagi–Sugeno fuzzy system with an application for a two-link robot control," *Proc. Inst. Mech. Eng., C, J. Mech. Eng. Sci.*, vol. 228, no. 9, pp. 1488–1500, Jun. 2014.

[27] M. R. Soltanpour and M. H. Khooban, "A particle swarm optimization approach for fuzzy sliding mode control for tracking the robot manipulator," *Nonlinear Dyn.*, vol. 74, nos. 1–2, pp. 467–478, Oct. 2013.

[28] Y.-K. Liu, N. Chao, H. Xia, M.-J. Peng, and A. Ayodeji, "Virtual reality-based adaptive dose assessment method for arbitrary geometries in nuclear facility decommissioning," *J. Radiological Protection*, vol. 38, no. 3, pp. 951–966, Sep. 2018.

[29] J. Byon, S. Park, Y. Kim, and S. Ahn, "External exposure specific analysis for radiation worker in reuse of containment building for Kori Unit 1," *Nucl. Eng. Technol.*, vol. 54, no. 5, pp. 1781–1788, May 2022.

[30] S. J. Park, J. Byon, D. H. Ban, S. Lee, W. Sohn, and S. Ahn, "Derivation of preliminary derived concentration guideline level (DCGL) by reuse scenario for Kori Unit 1 using RESRAD-BUILD," *Nucl. Eng. Technol.*, vol. 52, no. 6, pp. 1231–1242, Jun. 2020.

[31] N. Chao, Y.-K. Liu, H. Xia, A. Ayodeji, and L. Bai, "A dose assessment method for arbitrary geometries with virtual reality in the nuclear facilities decommissioning," *Radiat. Phys. Chem.*, vol. 144, pp. 238–247, Mar. 2018.



HAMZA KHAN received the B.S. degree in mechatronics engineering from Air University, Islamabad, Pakistan, in 2018, and the M.S. degree in mechanical engineering from Pusan National University, Busan, South Korea, in 2021, where he is currently pursuing the Ph.D. degree in mechanical engineering. His research interests include linear/nonlinear control, force control, robot manipulators kinematics, dynamics, and system identification.



JINWON LEE received the B.S. degree in computer engineering from Changwon National University, Changwon, South Korea, in 2020, and the M.S. degree in mechanical engineering from Pusan National University, Busan, South Korea, in 2022. His research interests include the design of virtual simulator and the implementation of robot in simulator.



JAEHYUNG KIM received the B.S. and M.S. degrees in mechanical engineering from Pusan National University, Busan, South Korea, in 2019 and 2021, respectively, where he is currently pursuing the Ph.D. degree in mechanical engineering. His research interests include intelligent robot control, kinematics, machine learning, machine vision, path planning, and autonomous robots and simulation.



MIN CHEOL LEE (Member, IEEE) received the B.S. degree in mechanical engineering from Pusan National University, Busan, South Korea, in 1983, and the M.Eng. degree in engineering science and the Ph.D. degree in applied physics from the University of Tsukuba, Tsukuba, Japan, in 1988 and 1991, respectively. In 1991, he joined the School of Mechanical Engineering, Pusan National University, where he has been a Professor, since 2002. His research interests include mechatronics, sliding mode control, medical robotics, and navigation/localization of mobile robots.



CHENGQIAN LI received the B.S. degree in mechanical engineering from Pusan National University, Busan, South Korea, in 2021, where he is currently pursuing the M.S. degree in mechanical engineering. His research interests include robot manipulators kinematics and dynamics, linear/nonlinear control, intelligent control, system identification, and robust and adaptive control.

...